Biochemical and Biophysical Research Communications 510 (2019) 442–448

Contents lists available at ScienceDirect

Biochemical and Biophysical Research Communications

journal homepage: www.elsevier.com/locate/ybbrc

Characterizing the structural and thermodynamic properties of Aβ42 and Aβ40

Yuxi Lin, Haeri Im, Le Thi Diem, Sihyun Ham*

Department of Chemistry, The Research Institute of Natural Sciences, Sookmyung Women's University, Cheongpa-ro-47-gil 100, Yongsan-ku, Seoul, 04310, South Korea

ARTICLE INFO

Article history:
Received 22 January 2019
Accepted 28 January 2019
Available online 2 February 2019

Keywords:
Protein aggregation
Amyloid beta protein
Molecular dynamics simulation
Solvation free energy

ABSTRACT

The self-assembly of amyloid-beta (Aβ) proteins in aqueous extracellular environments is implicated in Alzheimer's disease. Among several alloforms of Aβ proteins differing in sequence length, the 42- and 40-residue forms (Aβ42 and Aβ40) are the most abundant ones in the human body. Although the only difference is the additional $I_{41}A_{42}$ residues in the C-terminus, Aβ42 exhibits more aggregation tendency and stronger neurotoxicity than Aβ40. Here, we investigate the molecular factors that confer more aggregation potential to Aβ42 than to Aβ40 based on molecular dynamics simulations combined with solvation thermodynamic analyses. It is observed that the most salient structural feature of Aβ42 relative to Aβ40 is the more enhanced β-sheet forming tendency, in particular in the C-terminal region. While such a structural characteristic of Aβ42 will certainly serve to facilitate the formation of aggregate species rich in β-sheet structure, we also detect its interesting thermodynamic consequence. Indeed, we find from the decomposition analysis that the C-terminal region substantially increases the solvation free energy (i.e., overall "hydrophobicity") of Aβ42, which is caused by the dehydration of the backbone moieties showing the enhanced tendency of forming the β-structure. Together with the two additional hydrophobic residues ($I_{41}A_{42}$), this leads to the higher solvation free energy of Aβ42, implying the larger water-mediated attraction toward the self-assembly. Thus, our computational results provide structural and thermodynamic grounds on why Aβ42 has more aggregation propensity than Aβ40 in aqueous environments.

1. Introduction

Amyloid-beta (Aβ) proteins are the major component of extracellular aggregates found in the brain of Alzheimer's disease (AD) patients [1]. These proteins are produced from the amyloid-beta precursor protein through the cleavage by the β- and γ-secretases. The resulting Aβ alloforms are composed of different sequence lengths ranging from 36 to 43 residues. About 90% of the Aβ production from the cells is Aβ40 and the remainder is almost Aβ42 (~10%). While they differ only in the C-terminus ($I_{41}A_{42}$), they exhibit distinct biophysical, physiological, and clinical characteristics [2,3]. In particular, Aβ42 aggregates much faster and easily compared to Aβ40, and its neurotoxicity is stronger [2]. In addition, Aβ42 is found to be more abundant in the brains of AD patients [4].

Deducing why Aβ42 is more aggregation prone than Aβ40 requires detailed studies on the respective monomers to identify factors facilitating their interconversions to oligomers and amyloid fibrils. However, while the structural studies on oligomers and amyloid fibrils have been much advanced in recent years [5–7], experimental determination of the monomer structure has been hampered by their intrinsically disordered nature and strong propensity to aggregate in aqueous environments [8]. Computer simulations have therefore played a complementary role, in particular, for elucidating distinctive characteristics of Aβ42 and Aβ40 monomers [9]. However, key structural and thermodynamic traits that capture distinct aggregation propensity of Aβ42 and Aβ40 remain elusive.

Herein, we report computational studies to explore distinctive structural and thermodynamic characteristics of Aβ42 and Aβ40 monomers in aqueous environments. We performed explicit-water MD simulations to analyze the structural differences between Aβ42 and Aβ40. Solvation free energy calculations using the liquid integral-equation theory were also carried out to investigate the thermodynamic features of Aβ42 and Aβ40. Solvation free energy is

* Corresponding author.
E-mail address: sihyun@sookmyung.ac.kr (S. Ham).

https://doi.org/10.1016/j.bbrc.2019.01.124
0006-291X/

the key thermodynamic parameter dictating the protein aggregation propensity since it quantifies an overall affinity of a protein toward solvent water [10]: higher solvation free energy (i.e., less favorable solvation by water) of a protein implies more aggregation-prone potential. To uncover the origin of the difference in solvation free energy between Aβ42 and Aβ40, we also performed its decomposition analysis [11] which allows us to investigate how the structural and thermodynamic properties are connected. Thereby, we aim to uncover the structural and thermodynamic factors relevant to the distinct aggregation propensity exhibited by these proteins.

2. Materials and methods

2.1. Molecular dynamics simulations

We used the PMEMD module in the AMBER16 simulation suite [12] to conduct explicit-water MD simulations for Aβ42 and Aβ40. For proteins, we adopted the ff99SB force field [13], whereas for water we applied the TIP4P-Ew model [14]. Aβ42 (Aβ40) protein was solvated by counter ions and 13,419 (10,496) water molecules in a cubic box of the size ~75 Å (~69 Å). Since both Aβ42 and Aβ40 monomers are inherently disordered in aqueous media, we carried out the heating/annealing simulations [15] prior to the production runs. The production runs were performed at an ambient condition (300 K and 1 bar) using Berendsen's method [16]. Twelve independent 100 ns production runs were carried out for each of Aβ42 and Aβ40 proteins. From the Aβ42 and Aβ40 simulation trajectories, we saved protein conformations every after 5 ps for the structural analyses. The *J*-coupling constants were computed using the Karplus equation [17]. The contents of the secondary structure were analyzed with the DSSP program [18]. The main-chain and side-chain contact maps were created based on the heavy atoms contacts, which were considered formed if the distance between them is lower than 7 Å. Representative protein structures were obtained by performing the RMSD-based K-clustering analysis (4.0 Å cutoff) [19].

2.2. Solvation free energy analyses

We computed the solvation free energy G_{solv} using the 3D-RISM (three-dimensional reference interaction site model) theory [20]. Each-residue contribution to G_{solv} was obtained based on the exact atomic decomposition method [11]. We notice here a major drawback of the 3D-RISM, which is its poor ability to accurately compute *absolute* values of G_{solv}. On the other hand, it is known that *relative* values are reasonably accurate due to the cancellation of errors [10]. In the present work, we are primarily interested in the difference in solvation free energy, $\Delta G_{solv} = G_{solv}(A\beta42) - G_{solv}(A\beta40)$, of Aβ42 and Aβ40 and its decomposition into contributions from constituent residues. The mentioned drawback of the 3D-RISM matters here because of the difference in sequence length, in particular, in the C-terminus contribution to ΔG_{solv}, defined here as $\Delta G_{C\text{-terminus}} = G_{solv}(V_{40}I_{41}A_{42}) - G_{solv}(V_{40})$ in terms of the last three residues ($V_{40}I_{41}A_{42}$) of Aβ42 and the last residue (V_{40}) of Aβ40. Recently, an empirical model has been proposed that aims to correct G_{solv} from the 3D-RISM [21], which was adopted here to estimate the correction to the C-terminus contribution.

3. Results and discussion

3.1. Validation through experimental data

Aβ42 and Aβ40 monomers in aqueous solutions are intrinsically disordered lacking a well-defined three-dimensional structure. To validate the simulated structures of disordered proteins, the comparison with NMR experiments is common and useful. Such validation is presented in Fig. 1A, where we compare the simulated *J*-

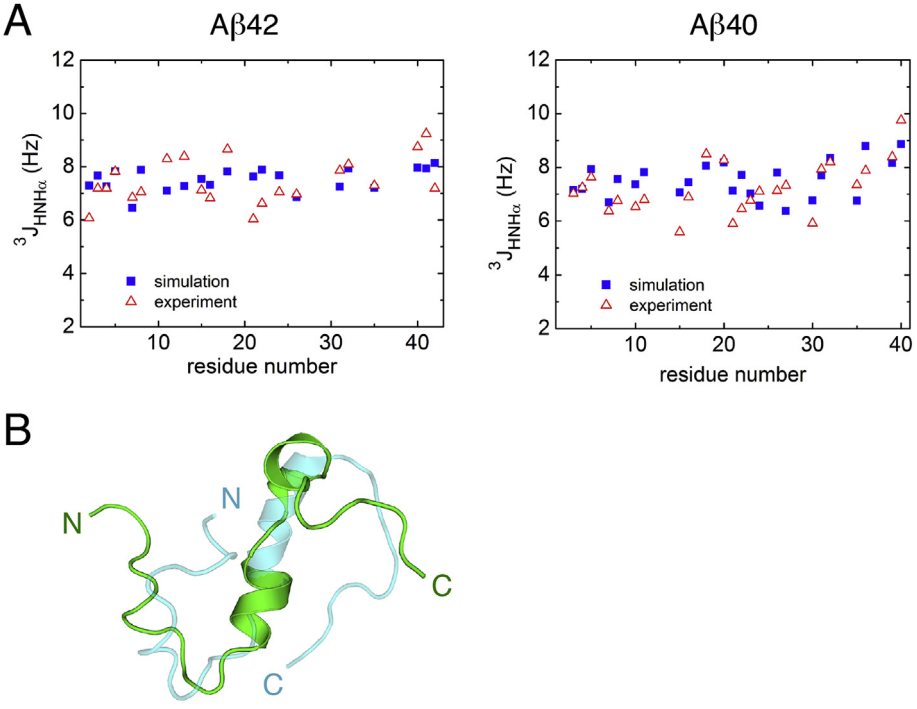

Fig. 1. (A) Simulated *J*-coupling constants (blue squares) and the NMR data (red triangles) for Aβ42 (left panel) and Aβ40 (right panel). (B) Simulated structure (green; the representative structure determined from the clustering analysis) and experimental structure (cyan) from an aqueous-phase NMR (PDB ID: 2LFM) for Aβ40. (For interpretation of the references to color in this figure legend, the reader is referred to the Web version of this article.)

coupling constants with the NMR data [22]. We find reasonable agreement both for Aβ42 and Aβ40. The average values of the simulated *J*-coupling constants are 7.5 Hz for both Aβ42 and Aβ40, whereas those of the experimental values are 6.8 Hz for Aβ42 and 6.6 Hz for Aβ40, i.e., the simulated values are higher than the experimental ones by ~10%. As recently pointed out [23], this difference may be partly due to the relaxation effects that would lead to ~10% upward shift of the experimental values.

Because of the intrinsically disordered nature in aqueous solutions, the atomic-level structure determination from experiments has been difficult for Aβ monomers. On the other hand, a recent NMR study reported an aqueous-solution structure for Aβ40, which exhibits the 3_{10}-helix structure in the residues 13–23 [24]. We found that our simulations for Aβ40 generate a structure that is relatively close to this experimental structure (Fig. 1B), showing the 3_{10}-helix structure in the residues 14–17 and 19–22. (The Cα RMSD value between the experimental and simulated structures is 2.6 Å for the residues 14–22, but it is 1.7 Å if the residues 14 and 17 exhibiting the largest deviations are excluded.) However, this particular Aβ40 structure was not stable in our simulations. Indeed, the cluster (with the cutoff value of 4.0 Å) that includes this structure populated only 1.5% of the trajectory. Although this might be caused by the inaccuracy of the force field, our simulations demonstrating no stable Aβ40 structure are consistent with the well-accepted view that Aβ40 monomer is inherently unstructured in aqueous environments. On the other hand, the structure shown Fig. 1B can be considered as a representative Aβ40 structure in the sense that the most distinctive structural characteristic of Aβ40 is the enhanced population of the 3_{10}-helix conformation in the residue region 14–17 (see blow).

3.2. Structural characteristics

The secondary-structure contents for Aβ42 and Aβ40 are displayed in Fig. 2, and Table 1 summarizes the averages over the whole sequence. Reflecting the intrinsically disordered nature, the secondary-structure contents of both Aβ42 and Aβ40 are dominated by turns (~17%) and coils (~70%). However, we do observe distinctive structural characteristics of these two proteins. We find that the β-sheet contents of Aβ42 are much higher than those of Aβ40 (Fig. 2C and G). On the other hand, while the α-helix contents for both proteins are low and comparable (~2%), the 3_{10}-helical structures are much more populated in Aβ40 than in Aβ42, in particular, in the residues 14–17 (Fig. 2B and F).

The intrinsically disordered characters of Aβ42 and Aβ40 are also reflected in somewhat large standard deviations of the secondary-structure contents (Table 1). To further investigate the nature of those large standard deviations, we show in Fig. 2D and H the population maps of the 3_{10}-helical versus the β-sheet contents for Aβ42 and Aβ40, respectively. (Each point in these figures represents the population of individual protein structures possessing the specific 3_{10}-helical and β-sheet contents.) It is clear from these figures that the secondary-structure contents of Aβ42 and Aβ40 largely deviate from the normal distribution; the standard deviations reported in Table 1 should therefore be taken just as a rough measure of the magnitude of the fluctuations in the secondary-structure contents. Nevertheless, specific conformational preferences mentioned above – the higher population of the β-sheet structures in Aβ42 and that of the 3_{10}-helical structures in Aβ40 – are clearly discernible also from these population maps.

To analyze the distinctive structural characteristics in more detail, we show in Fig. 3A the contact and difference maps for the main chain (left-upper parts) and side chain (right-lower parts). We find that the most significant effect of the presence of the additional two residues ($I_{41}A_{42}$) in Aβ42 shows up in the C-terminal region where the residues 28–40 form more contacts both in the main chain and side chain (red box in Fig. 3A, termed region IV for later reference; the representative structure exhibiting these contacts is displayed in Fig. 3B). These contacts reflect the aforementioned higher β-sheet forming tendency of Aβ42 in the C-terminal region (Fig. 2C). For Aβ40, we observe the enhanced side-chain contacts in the residues 14–17 (purple box in Fig. 3A, termed region II; the representative structure showing these contacts is presented in Fig. 3C). These side-chain contacts are formed due to the enhanced 3_{10}-helix population in this residue region of Aβ40 (Fig. 2F). In addition, we observe in Aβ40 the enhanced hydrophobic contacts in the residue region 19–27, which are not observed in Aβ42 (blue box in Fig. 3A, termed region III; the representative structure having these contacts is shown in Fig. 3C).

3.3. Thermodynamic features

The strength of the protein-water interaction characterized by G_{solv} is one of the controlling factors of the aggregation propensity [10]. We computed the difference in solvation free energy, $\Delta G_{solv} = G_{solv}(A\beta42) - G_{solv}(A\beta40)$, to investigate the distinctive thermodynamics features of Aβ42 and Aβ40, and found that $G_{solv}(A\beta42)$ is significantly higher than $G_{solv}(A\beta40)$, $\Delta G_{solv} = 41.4 \pm 15.7$ kcal/mol (average ± standard error).

To uncover the origin of the difference in solvation free energy, we decomposed ΔG_{solv} into each-residue contribution (Fig. 4A). To ease the discussion, we grouped these residue contributions into the charged-residue contribution, non-charged residue contribution, and the C-terminus contribution (Table 2): the contribution from the non-charged residues is further partitioned into the regions I to IV for later convenience (see below). We find that the largest contribution (29.6 ± 1.3 kcal/mol) to ΔG_{solv} originates from the C-terminal end, i.e., from the additional two hydrophobic residues ($I_{41}A_{42}$) in Aβ42, although this value may be considerably overestimated due to the drawback of the 3D-RISM. Indeed, the correction based on Ref. [21] provides a much smaller estimate (3.9 ± 1.5 kcal/mol) on the C-terminus contribution. We also observe that the large standard error (15.7 kcal/mol) of ΔG_{solv} stems mostly from that of the charged-residue contribution (9.6 ± 12.5 kcal/mol). This is because the electrostatic interaction dominates the solvation free energy change [25,26], and hence, ΔG_{solv} is quite sensitive to the hydrogen-bond/salt-bridge formation involving charged residues. Indeed, it is observed that the sign of ΔG_{solv} for the charged residues (colored in Fig. 4A) correlates well with the difference in the fraction of the hydrogen-bonds and salt-bridges formed with those residues (Table 3). Because of the large standard error, however, the relevance of the charged-residue contribution is not conclusive.

To further analyze the non-charged residue contribution, in particular to make connection with the structural analyses presented in the previous subsection, we partitioned the amino acid sequence into the four regions (Fig. 4B and Table 2). The region I (residues 2–13) is the N-terminal region, and we found that the contribution to ΔG_{solv} from this region is rather small (1.1 ± 3.8 kcal/mol). The region II (residues 14–17) is the region where we observed that Aβ40 exhibits the enhanced 3_{10}-helix forming character (Fig. 2F) and concomitant side-chain contacts (Fig. 3C). The formation of these contacts accompanies the dehydration of this region: this provides a positive contribution to $G_{solv}(A\beta40)$, and hence, a negative contribution to $\Delta G_{solv} = G_{solv}(A\beta42) - G_{solv}(A\beta40)$, whose value is found to be -2.3 ± 2.5 kcal/mol (Table 2). In the region III (residues 18–27), the enhanced formation of the hydrophobic contacts is found in Aβ40 relative to Aβ42 (Fig. 4B). This leads to a positive contribution to $G_{solv}(A\beta40)$, and therefore, a negative contribution to ΔG_{solv}, which is found to be -5.4 ± 3.5 kcal/mol.

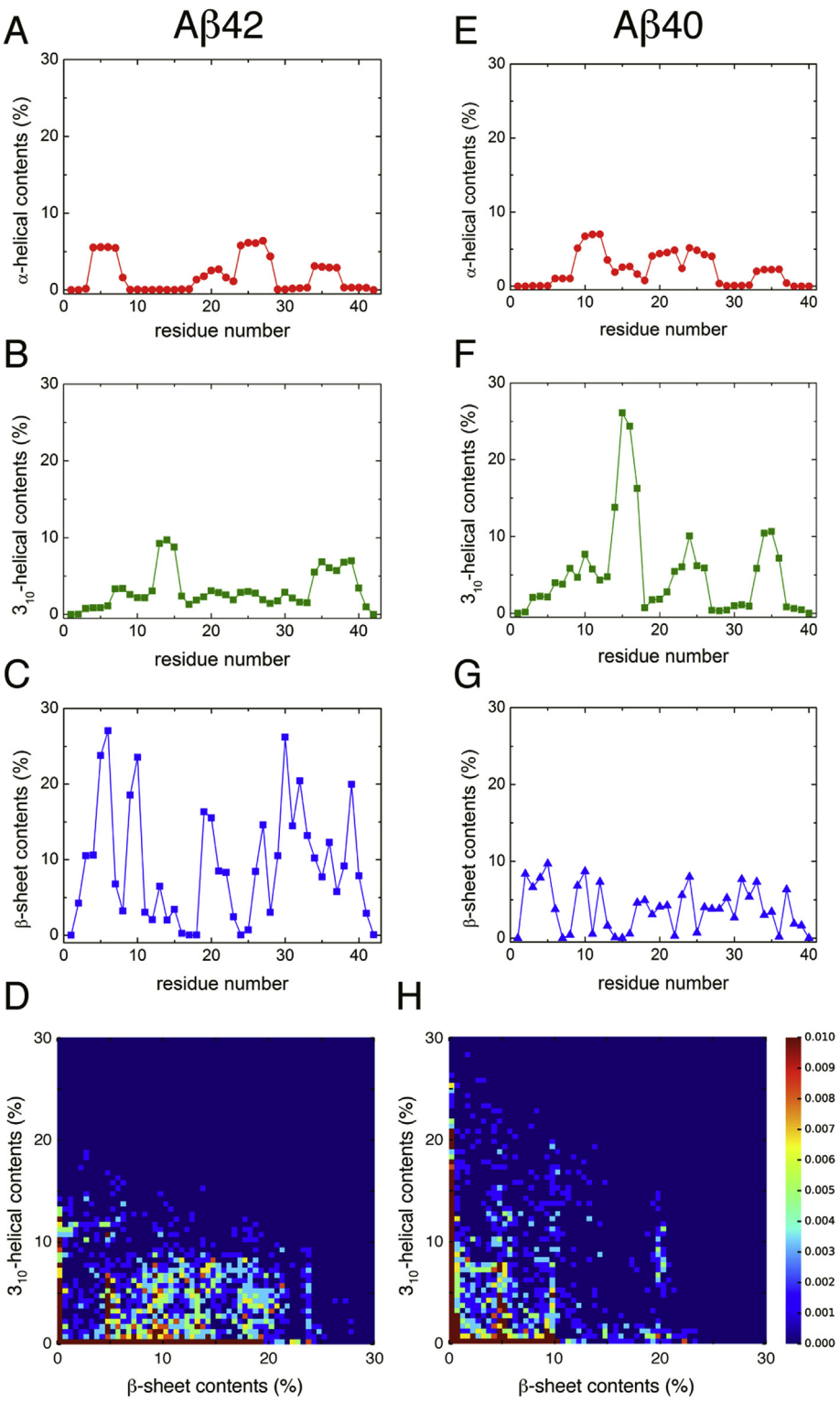

Fig. 2. (A–C) Average α-helix contents (A), 3_{10}-helix contents (B), and β-sheet contents (C) versus amino acid residue for Aβ42. (D) Population map of the 3_{10}-helical versus the β-sheet contents for Aβ42. (E–H) Corresponding results for Aβ40.

Table 1
Average secondary-structure content (%) ± standard deviation.

	α-helix	3_{10}-helix	β-sheet	Turn	Coil
Aβ42	1.9 ± 4.0	3.1 ± 4.9	9.1 ± 6.8	17.8 ± 8.8	68.1 ± 12.8
Aβ40	2.3 ± 5.4	5.2 ± 6.6	3.9 ± 5.3	16.1 ± 7.8	72.5 ± 12.5

Finally, the region IV (residues 29–39) is the C-terminal region where Aβ42 exhibits the enhanced β-sheet contents relative to Aβ40 (Figs. 2C and 4B). Because of the dehydration of this region, the region IV provides a positive contribution (+8.8 ± 3.9 kcal/mol) to ΔG_{solv}, whose magnitude is statistically meaningful and rather large.

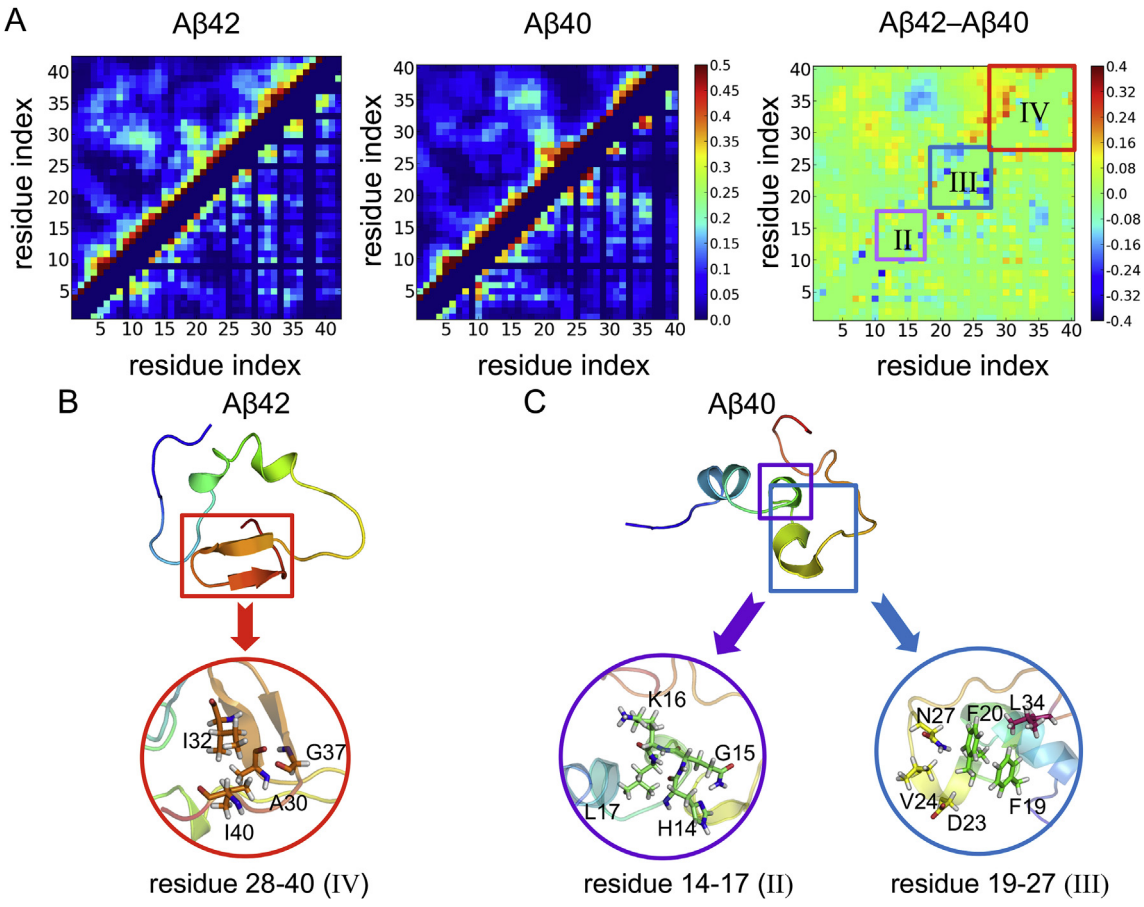

Fig. 3. (A) Intramolecular contact maps (fractions of the contacts formed) for Aβ42 and Aβ40, and the difference map (fractions for Aβ42 minus those for Aβ40). The left-upper parts refer to the main chain-main chain contacts, whereas the right-lower parts to the side chain-side chain contacts. In the difference map, the enhanced contacts formed by the residues 28–40 of Aβ42 are indicated by the red box, whereas the enhanced contacts formed by the residues 19–27 and 14–17 of Aβ40 are indicated by the purple and blue boxes, respectively. Representative Aβ42 (B) and Aβ40 (C) structures determined from the clustering analysis that exhibit these enhanced contacts. (For interpretation of the references to color in this figure legend, the reader is referred to the Web version of this article.)

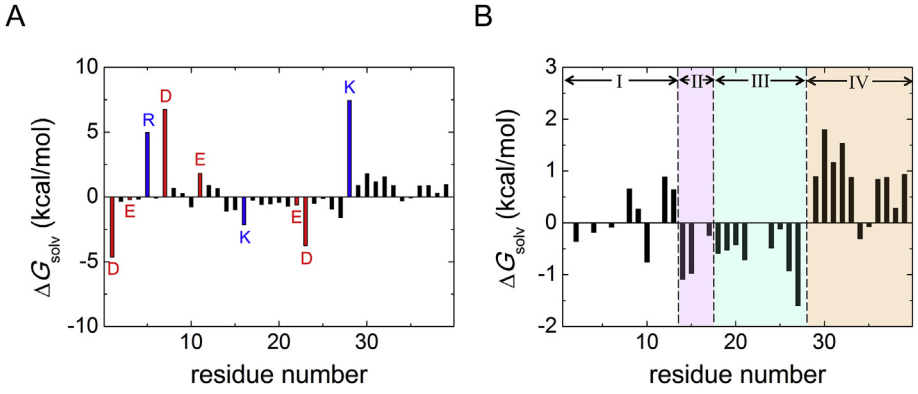

Fig. 4. (A) Each-residue contribution (from residues 1 to 39) to the solvation free energy difference, $\Delta G_{solv} = G_{solv}(A\beta42) - G_{solv}(A\beta40)$. Contributions from the positively (negatively) charged residues are colored blue (red), whereas those from the non-charged residues are drawn with black. (B) Magnified representation of the non-charged residue contributions to ΔG_{solv}. The sequence is divided into the region I (residues 2–13), II (14–17, colored light purple), III (18–27, light blue), and IV (29–39, light orange). (For interpretation of the references to color in this figure legend, the reader is referred to the Web version of this article.)

3.4. Molecular factors determining distinct aggregation propensity

The first step toward understanding why Aβ42 and Aβ40 proteins, despite only the tiny difference in the C-terminus, exhibit the distinct aggregation behavior is to uncover distinctive structural characteristics of these proteins. We find from our simulations that the most salient structural feature of Aβ42 relative to Aβ40 is the enhanced β-sheet forming tendency, in particular, in the C-terminal region (Figs. 2 and 4). Our simulation results agree with the experimental observations that Aβ42 possesses the C-terminal region which is more rigid and prone to form β-structure than Aβ40 [27,28]. In this regard, we notice that the larger β-sheet forming

Table 2
The charged and non-charged residue contributions to the solvation free energy difference ΔG_{solv} (in kcal/mol) ± standard error.

Charged residues	Non-charged residues				C-terminus ($V^{40}I^{41}A^{42}{}_{A\beta42} - V^{40}{}_{A\beta40}$)
	Region I	Region II	Region III	Region IV	
9.6 ± 12.5	1.1 ± 3.8	−2.3 ± 2.5	−5.4 ± 3.5	8.8 ± 3.9	29.6 ± 1.3 (3.9 ± 1.5)[a]

[a] After the correction based on Ref. [21].

Table 3
Average fraction (%) ± standard error with which each charged residue participates in the hydrogen-bond/salt-bridge formation.

	Aβ42	Aβ40	Difference
ASP1	84.9 ± 2.3	87.3 ± 2.4	−2.4 ± 3.3
GLU3	49.1 ± 7.5	53.7 ± 5.6	−4.6 ± 9.4
ARG5	76.3 ± 4.6	65.9 ± 4.3	10.3 ± 6.3
ASP7	86.8 ± 2.2	83.0 ± 1.6	3.8 ± 2.7
GLU11	29.6 ± 6.1	32.6 ± 5.3	−3.0 ± 8.0
LYS16	33.5 ± 6.1	38.8 ± 6.1	−5.3 ± 8.6
GLU22	24.9 ± 6.2	20.8 ± 3.1	4.1 ± 6.9
ASP23	85.1 ± 2.9	89.9 ± 2.5	−4.8 ± 3.8
LYS28	38.8 ± 6.3	25.2 ± 2.4	13.6 ± 6.7

propensity has been suggested as one of the key factors determining the aggregation propensity [29,30]. Thus, the enhanced β-sheet forming propensity of the C-terminal region of Aβ42 compared to Aβ40 provides the structural ground for the higher aggregation potential of Aβ42, acting to facilitate the formation of oligomers and fibrils rich in β-sheet structure.

The relevance of water-induced interaction in protein aggregation has also been suggested [31,32]. In particular, the solvation free energy quantifying the strength of the water-mediated force has been demonstrated as the relevant factor determining the protein aggregation propensity [10]. In consistent with this picture, the overall hydrophobicity (solvation free energy) of Aβ42 is found to be much higher than that for Aβ40, implying that the surrounding water imparts a larger water-mediated attraction for the self-assembly of Aβ42. The decomposition analysis furthermore indicates that, while the presence of extra hydrophobic residues ($I_{41}A_{42}$) in the C-terminal end mainly accounts for the increased hydrophobicity of Aβ42 over Aβ40, the enhanced β-structure forming tendency in the C-terminal is also responsible for this thermodynamic feature. Thus, our computational results provide consistent and connected structural and thermodynamic bases for the higher aggregation potential of Aβ42, which are largely rooted in the C-terminal region. This is in agreement with the experimental implication that this region of Aβ42 may be the seed for aggregation [29,33,34].

In conclusion, we report computational studies on Aβ42 and Aβ40 associated with Alzheimer's disease based on the MD simulations and on the solvation thermodynamic analyses, exploring the structural and thermodynamic origin on why Aβ42 aggregates much faster than Aβ40. We observe that Aβ42 exhibits the higher tendency of forming β-sheet conformations than Aβ40, which will facilitate the conversion toward β-sheet rich oligomer species and amyloid fibrils. We also find from the solvation thermodynamic analysis that the Aβ42 is more hydrophobic than Aβ40, implying that the larger water-mediated attraction will operate for the self-assembly of Aβ42. The increased hydrophobicity of Aβ42 not only originates from the additional two hydrophobic residues ($I_{41}A_{42}$) at the C-terminus, but is also contributed from the enhanced tendency for forming the β-structure in the C-terminal region. Thus, our work offers a structurally and thermodynamically consistent picture on why Aβ42 exhibits a more aggregation-prone nature than Aβ40.

Conflicts of interest

All authors declare no conflicts of interest.

Acknowledgments

This research was supported by the Sookmyung Women's University Research Grants (1-1503-0241).

Transparency document

Transparency document related to this article can be found online at https://doi.org/10.1016/j.bbrc.2019.01.124

References

[1] M. Goedert, M.G. Spillantini, A century of Alzheimer's disease, Science 314 (2006) 777–781.
[2] J.T. Jarrett, E.P. Berger, P.J. Lansbury Jr., The carboxy terminus of the β amyloid protein is critical for the seeding of amyloid formation: implications for the pathogenesis of Alzheimer's disease, Biochemistry 32 (1993) 4693–4697.
[3] K. Murakami, K. Irie, A. Morimoto, H. Ohigashi, M. Shindo, M. Nagao, T. Shimizu, T. Shirasawa, Neurotoxicity and physicochemical properties of Aβ mutant peptides from cerebral amyloid angiopathy, J. Biol. Chem. 278 (2003) 46179–46187.
[4] H. Fukumoto, A. Asami-Odaka, N. Suzuki, H. Shimada, Y. Ihara, T. Iwatsubo, Amyloid beta protein deposition in normal aging has the same characteristics as that in Alzheimer's disease, Am. J. Pathol. 148 (1996) 259–265.
[5] L. Gu, C. Liu, J.C. Stroud, S. Ngo, L. Jiang, Z. Guo, Antiparallel triple-strand architecture for prefibrillar Aβ42 oligomers, J. Biol. Chem. 289 (2014) 27300–27313.
[6] Y. Xiao, B. Ma, D. McElheny, S. Parthasarathy, F. Long, M. Hoshi, R. Nussinov, Y. Ishii, Aβ(1–42) fibril structure illuminates self-recognition and replication of amyloid in Alzheimer's disease, Nat. Struct. Mol. Biol. 22 (2015) 499–505.
[7] M.T. Colvin, R. Silvers, B. Frohm, Y. Su, S. Linse, R.G. Griffin, High resolution structural characterization of $A\beta_{42}$ amyloid fibrils by magic angle spinning NMR, J. Am. Chem. Soc. 137 (2015) 7509–7518.
[8] D.B. Teplow, Preparation of amyloid beta-protein for structural and functional studies, Methods Enzymol. 413 (2006) 20–33.
[9] J. Nasica-Labouze, P.H. Nguyen, F. Sterpone, O. Berthoumieu, N.-V. Buchete, S. Coté, A. De Simone, A.J. Doig, P. Faller, A. Garcia, A. Laio, M.S. Li, S. Melchionna, N. Mousseau, Y. Mu, A. Paravastu, S. Pasquali, D.J. Rosenman, B. Strodel, B. Tarus, J.H. Viles, T. Zhang, C. Wang, P. Derreumaux, Amyloid β protein and Alzheimer's disease: when computer simulations complement experimental studies, Chem. Rev. 115 (2015) 3518–3563.
[10] S.-H. Chong, S. Ham, Interaction with the surrounding water plays a key role in determining the aggregation propensity of proteins, Angew. Chem. Int. Ed. 53 (2014) 3961–3964.
[11] S.-H. Chong, S. Ham, Atomic decomposition of the protein solvation free energy and its application to amyloid-beta protein in water, J. Chem. Phys. 135 (2011), 034506.
[12] D.A. Case, et al., AMBER 16, University of California, San Francisco, 2016.
[13] V. Hornak, R. Abel, A. Okur, B. Strockbine, A. Roitberg, C. Simmerling, Comparison of multiple Amber force fields and development of improved protein backbone parameters, Proteins 65 (2006) 712–725.
[14] H.W. Horn, W.C. Swope, J.W. Pitera, J.D. Madura, T.J. Dick, G.L. Hura, T. Head-Gordon, Development of an improved four-site water model for biomolecular simulations: TIP4P-Ew, J. Chem. Phys. 120 (2004) 9665–9678.
[15] S.-H. Chong, J. Yim, S. Ham, Structural heterogeneity in familial Alzheimer's disease mutants of amyloid-beta peptides, Mol. Biosyst. 9 (2013) 997–1003.
[16] H.J.C. Berendsen, J.P.M. Postma, W.F. van Gunsteren, A. DiNola, J.R. Haak, Molecular dynamics with coupling to an external bath, J. Chem. Phys. 81 (1984) 3684–3690.
[17] M. Karplus, Contact electron-spin coupling of nuclear magnetic moments, J. Chem. Phys. 30 (1959) 11–15.
[18] W. Kabsch, C. Sander, Dictionary of protein secondary structure: pattern recognition of hydrogen-bonded and geometrical features, Biopolymers 22 (1983) 2577–2637.
[19] M. Feig, J. Karanicolas, C.L. Brooks, MMTSB tool set: enhanced sampling and

multiscale modeling methods for applications in structural biology, J. Mol. Graph. Model. 22 (2004) 377–395.
[20] T. Imai, Y. Harano, M. Kinoshita, A. Kovalenko, F. Hirata, A theoretical analysis on hydration thermodynamics of proteins, J. Chem. Phys. 125 (2006), 024911.
[21] D.S. Palmer, A.I. Frolov, E.L. Ratkova, M.V. Fedorov, Towards a universal method for calculating hydration free energies: a 3D reference interaction site model with partial molar volume correction, J. Phys. Condens. Matter 22 (2010) 492101.
[22] N.G. Sgourakis, Y. Yan, S.A. McCallum, C. Wang, A.E. Garcia, The Alzheimer's peptides Abeta40 and 42 adopt distinct conformations in water: a combined MD/NMR study, J. Mol. Biol. 368 (2007) 1448–1457.
[23] A.K. Ball, A.H. Phillips, D.E. Wemmer, T. Head-Gordon, Differences in β-strand populations of monomeric Aβ40 and Aβ42, Biophys. J. 104 (2013) 2714–2724.
[24] S. Vivekanandan, J.R. Brender, S.Y. Lee, A. Ramamoorthy, Biochem. A partially folded structure of amyloid-beta(1–40) in an aqueous environment, Biophys. Res. Commun. 411 (2011) 312–316.
[25] S.-H. Chong, C. Lee, M. Park, S. Ham, Structural and thermodynamic investigations on the aggregation and folding of acylphosphatase by molecular dynamics simulations and solvation free energy analysis, J. Am. Chem. Soc. 133 (2011) 7075–7083.
[26] S.-H. Chong, S. Ham, Site-directed analysis on protein hydrophobicity, J. Comput. Chem. 136 (2014) 12314–12322.
[27] L. Hou, H. Shao, Y. Zhang, H. Li, N.K. Menon, E.B. Neuhaus, J.M. Brewer, I.-J.L. Byeon, D.G. Ray, M.P. Vitek, T. Iwashita, R.A. Makula, A.B. Przybyla, M.G. Zagorski, Solution NMR studies of the Aβ(1–40) and Aβ(1–42) peptides establish that the Met35 oxidation state affects the mechanism of amyloid formation, J. Am. Chem. Soc. 126 (2004) 1992–2005.
[28] Y. Yan, C. Wang, Abeta42 is more rigid than Abeta40 at the C terminus: implications for Abeta aggregation and toxicity, J. Mol. Biol. 364 (2006) 853–862.
[29] F. Chiti, M. Stefani, N. Taddei, G. Ramponi, C.M. Dobson, Rationalization of the effects of mutations on peptide and protein aggregation rates, Nature 424 (2003) 805–808.
[30] A.B. Ahmed, A.V. Kajava, Breaking the amyloidogenicity code: methods to predict amyloids from amino acid sequence, FEBS Lett. 587 (2013) 1089–1095.
[31] M.G. Krone, L. Hua, P. Soto, R. Zhou, B.J. Berne, J.-E. Shea, Role of water in mediating the assembly of Alzheimer amyloid-β Aβ16–22 protofilaments, J. Am. Chem. Soc. 130 (2008) 11066–11072.
[32] G. Reddy, J.E. Straub, D. Thirumalai, Dry amyloid fibril assembly in a yeast prion peptide is mediated by long-lived structures containing water wires, Proc. Natl. Acad. Sci. U.S.A. 107 (2010) 21459–21464.
[33] A. Morimoto, K. Irie, K. Murakami, Y. Masuda, H. Ohigashi, M. Nagao, H. Fukuda, T. Shimizu, T. Shirasawa, Analysis of the secondary structure of β-amyloid (Aβ42) fibrils by systematic proline replacement, J. Biol. Chem. 279 (2004) 52781–52788.
[34] K.H. Lim, G.L. Henderson, A. Jha, M. Louhivuori, Structural, dynamic properties of key residues in Aβ amyloidogenesis: implications of an important role of nanosecond timescale dynamics, Chembiochem 8 (2007) 1251–1254.